Supplementary Information

Printable Nanoscale Metal Ring Arrays via Vertically Aligned Carbon Nanotube Platforms

Sang Ho Lee[a,b], Seungha Yoon[a], Huisu Jeong[a], Mingu Han[a], Sung Mook Choi[c], Jong Guk Kim[a,b], Ji-Woong Park[a], Gun Young Jung[a], Beong Ki Cho[a], and Won Bae Kim*[a,b]

[a] *School of Materials Science and Engineering, Gwangju Institute of Science and Technology (GIST), Gwangju 500-712, Republic of Korea.*

[b] *Research Institute for Solar and Sustainable Energies, Gwangju Institute of Science and Technology (GIST), Gwangju 500-712, Republic of Korea.*

[c] *Surface Technology Division, Korea Institute of Materials Science (KIMS), Changwon 641-010, Republic of Korea.*

Contents:

* Address correspondence to wbkim@gist.ac.kr.

4. **The effect of the ion milling process on the configuration of the CNT tips**
5. **SEM images of the Au metal-loaded CNT stamp**
6. **Confirmation of the release layers via contact angle measurement**
7. **AFM analysis of the printed Au nanorings on Al substrates**
8. **Confirmation of the Ti adhesion layers via XPS analysis**
9. **The large range of XRD inspections**
10. **LSPR of the printable Au nanodots and nanorings**

Fabrication process of the CNT arrays

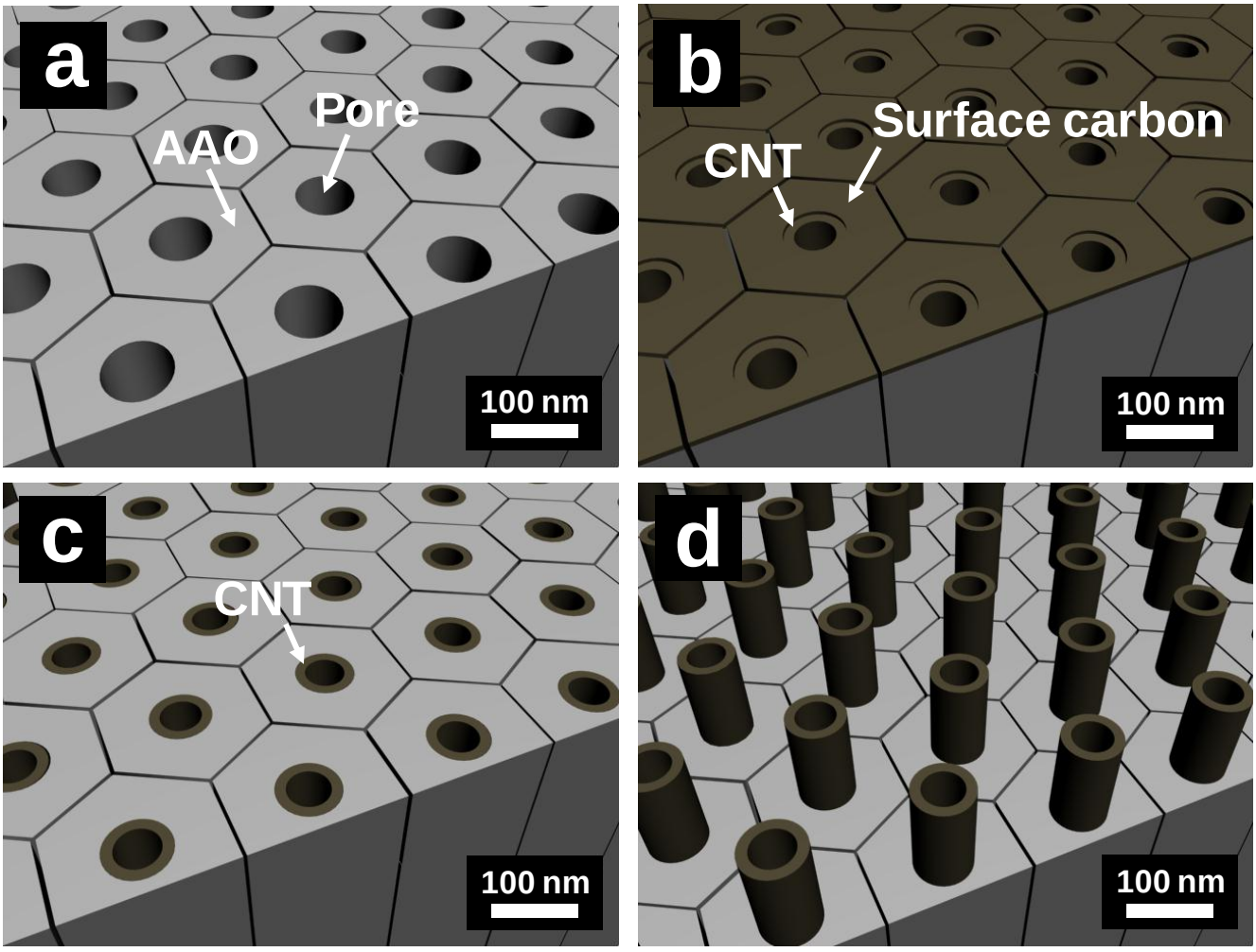

Figure S1. A schematic illustration of the fabrication procedures of the CNT stamp: (a) the preparation

of the nanoporous AAO template, (b) the deposition of the carbon layers within the AAO channels *via* the pyrolysis of a hydrocarbon source at 600 °C, (c) the removal of the surface carbon layer by the Ar ion milling process, and (d) the selective exposure of the vertical CNT arrays *via* chemical wet etching.

Reusability of the CNT stamps

Figure S2 shows a fresh CNT stamp, a stamp that has been reused five times, the Au nanoring arrays that were printed by the fresh stamp, and the Au nanorings that were printed by the reused stamp. Even after the repeated printing process, the tip morphology of the reused CNT arrays (Figure S2b) is maintained with minimal structural deformation, compared with that of the fresh arrays (Figure S2a), due to the homogeneous height of the high-density CNTs and to the flexibility of the one-dimensional carbon architecture. Although a few metal remnants are observed on the CNT tip due to the repetitive loading of metal layers on the stamps and to the consecutive printing process, the reused stamp tips still retain their ring configuration (Figure S2b). Figure S2d shows the Au nanoring arrays that were printed by the reused CNT stamp. The printed result is almost identical to the Au nanorings that were printed by the fresh CNT stamp (Figure S2c), indicating the reusability of our CNT stamps.

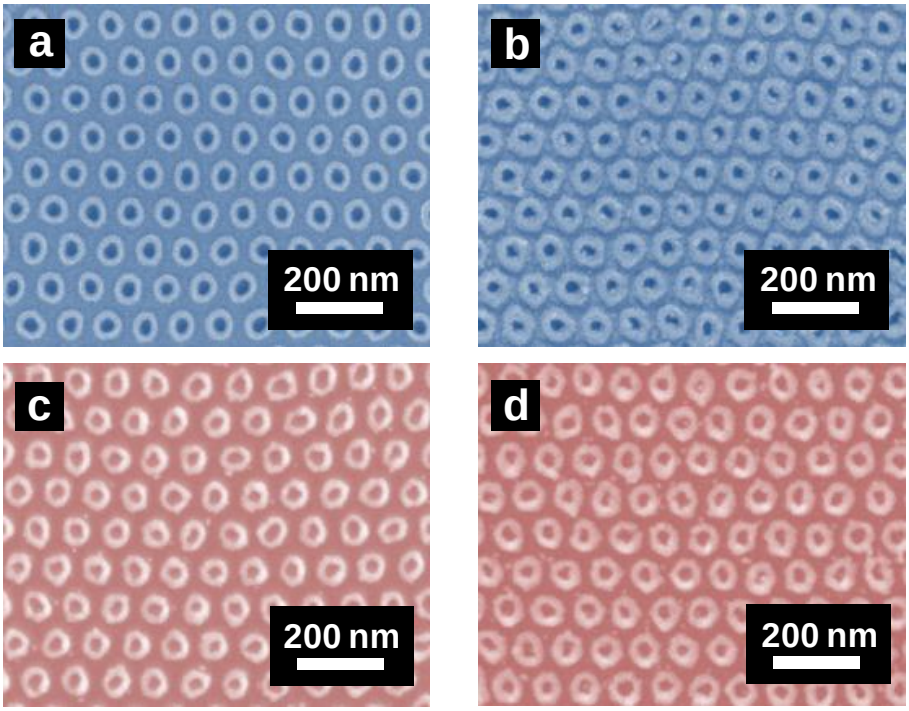

Figure S2. SEM images of (a) the pristine CNT stamp, (b) the stamp after contact printing, (c) the Au nanoring arrays that were printed by the fresh stamp, and (d) the Au nanorings that were printed by the used stamp. Here, the deposition of metal layers on the reused stamp was performed using the same process as that for the fresh stamp.

High-resolution TEM image of the CNT wall layers

The TEM images in Figure S3 show a detailed investigation of the wall morphology of the CNTs that were fabricated within the AAO templates. The CNTs exhibit a straight-line morphology and a hollow core part (Figure S3a), which is reproduced with complete fidelity to the AAO pore channels. The high-resolution TEM (HRTEM) image (Figure S3b) reveals that the tube wall is constructed of a stack of graphite flakes.

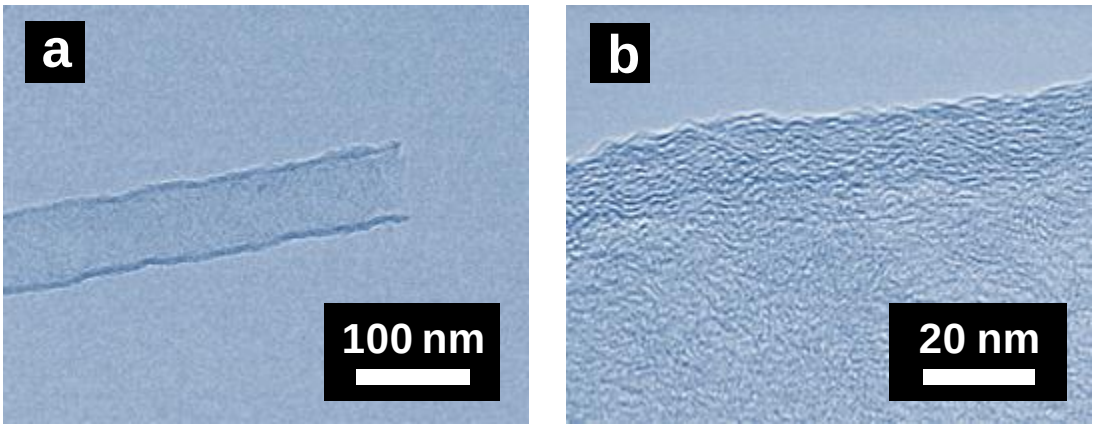

Figure S3. (a) TEM image of an individual CNT that was extracted from the AAO templates. (b) HRTEM images of the CNT wall layer, which consists of a stack of graphite flakes.

The effect of the ion milling process on the configuration of the CNT tips

The SEM images in Figure S4 show the changes in the morphologies of the CNT tips with varying ion milling time. Here, the electron beam current and acceleration current are constantly maintained during the ion milling process, and, after this process, all of the samples are chemically etched in the prepared etching solution for the same etching time. An incomplete ion milling process results in CNT arrays with connected and un-isolated tips (Figure S4a), whereas an ion milling process longer than the proper time appears to produce crumbled (Figure S4c) or closed-end tips (Figure S4d). Additionally, the protruded height of each CNT array sample exhibits a slight difference (the lower part of the SEM images), even if the selective exposure of all of the CNT arrays due to the chemical etching of the AAO templates occurs under the same condition. This phenomenon might be attributed to the collapse of the CNT ends due to the different ion milling conditions. The arrays with imperfect ends cannot be an efficient platform for the printing of nanoring arrays.

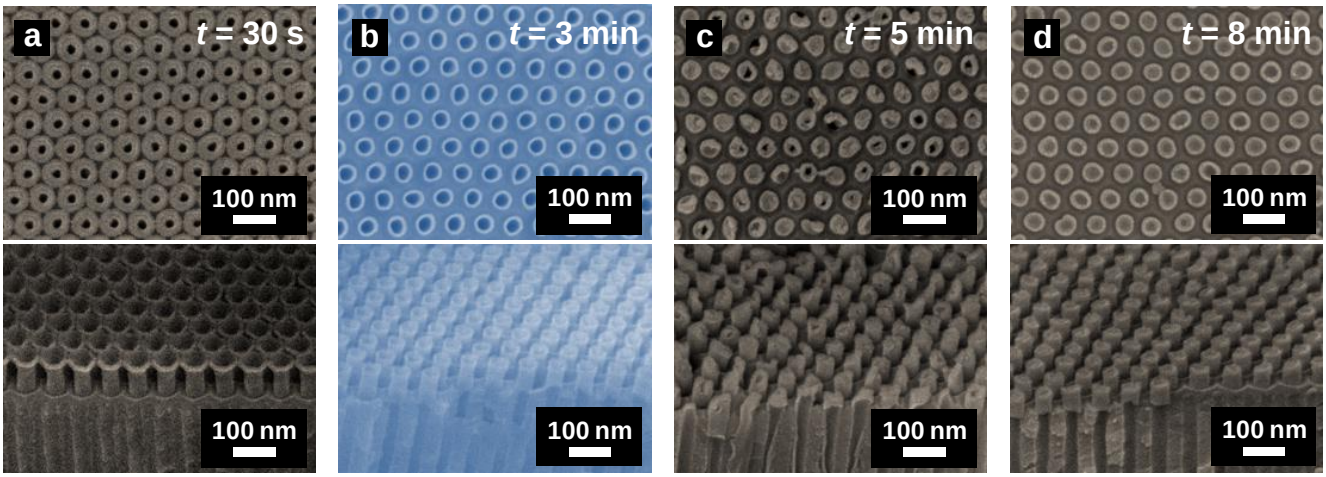

Figure S4. SEM images of the CNT arrays with different tip morphologies. The photographs in the upper parts show a top-view of the stamping arrays, while the images in the lower parts display a tilted view. The pore diameter and channel depth of the AAO templates that were used in this experiment are identical, and the deposition conditions of the carbon layers within the AAO pores are also the same for all samples.

SEM images of the Au metal-loaded CNT stamp

The SEM images in Figure S5 show the Au metal-loaded CNT stamps. Au metal layers (approximately 12 nm) were preliminarily deposited on the CNT tips, which were pre-coated with anti-sticking monolayers, and adhesion-enhancing Ti layers (approximately 1 nm) were then consecutively loaded onto the Au layers by E-beam or thermal evaporation. After the deposition of the metal layers on the tips, the ring-shaped CNT tips were still maintained (Figure S5a). From the cross-sectional SEM image (Figure S5b), it can be confirmed that the deposition of the metal layers on the isolated tips of the CNT arrays was achieved without disturbing the original configuration of the stamp tips.

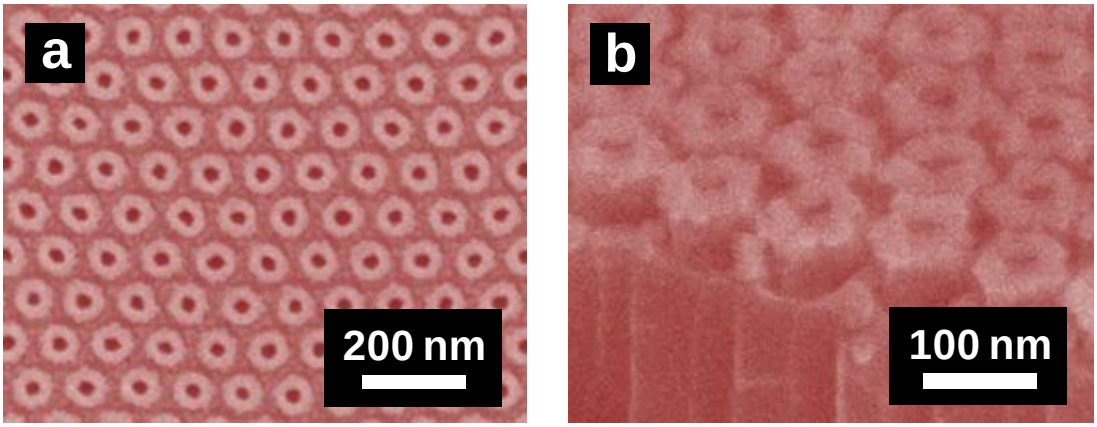

Figure S5. SEM images of a (a) top-view and (b) cross-sectional view of the metal-loaded CNT stamp. The average tip size of the CNTs that were used in this experiment is approximately 65 nm, and the protruded height of the CNT arrays from the AAO surfaces is approximately 60 nm.

Confirmation of the release layers via contact angle measurement:

The existence of the release layers $CF_3(CF_2)_5(CH_2)_2SiCl_3$ (tridecafluoro-1,1,2,2-tetrahydrooctyl-trichlorosilane) on the CNT stamps was investigated by measuring the water contact angle. We found that the contact angle of the CNT stamp with the release layers was much larger than that of the stamps without the layers (see the Table S1 and Figure S6), which should be attributed to the presence of fluorocarbon functional groups of the releasing molecules. The difference in the water contact angle clearly indicates the existence of the release layers on the stamp surfaces.

Table S1. Water contact angle measurement of the CNT stamps with and without the release layers.

Sample preparation	Contact angle (degree)
CNT stamp w/o release layers	49.1
CNT stamp w/ release layers	92.1

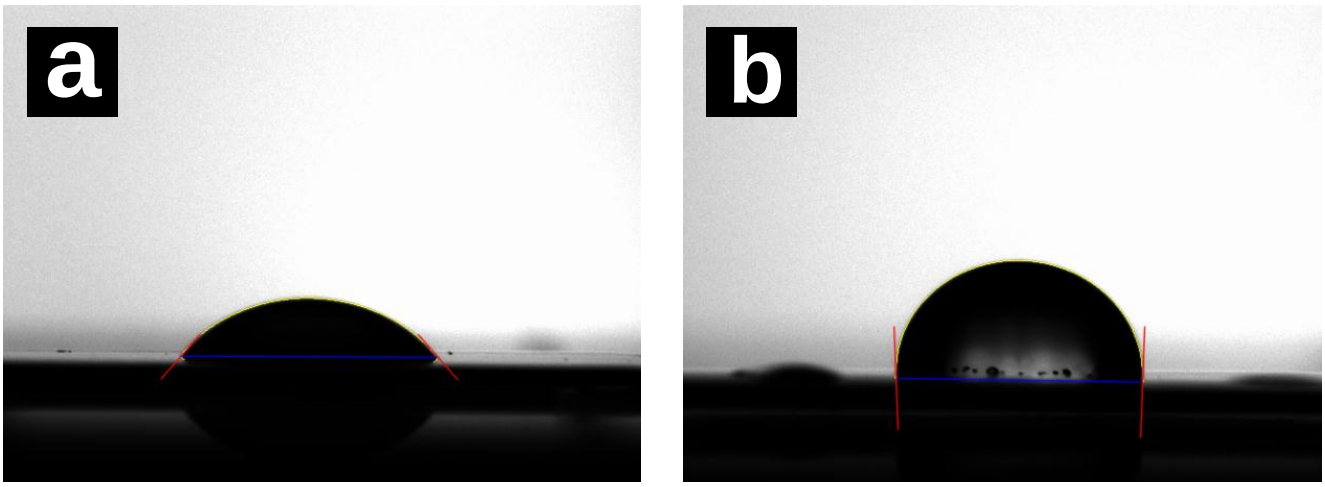

Figure S6. Photograph images of water droplets that were dropped to the CNT stamps (a) without release layers and (b) with release layers.

AFM analysis of the printed Au nanorings on Al substrates:

Figure S7 shows the AFM data of the Au nanorings printed on Al substrates, which displays *ca.* 66 nm in their outer diameter. From the AFM data, the height of the printed nanorings is estimated to *ca.* 20 ± 3 nm. This value shows quite reasonable correspondence with the ring height observed from SEM analysis.

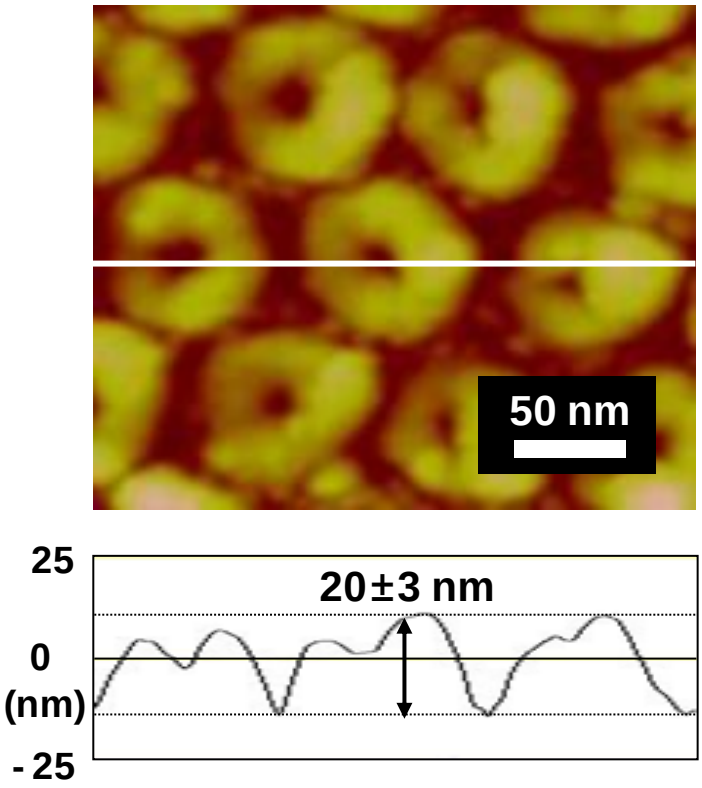

Figure S7. Height-contrast AFM results of the Au nanoring arrays printed on Al substrates.

Confirmation of the Ti adhesion layers via XPS analysis:

The existence of the Ti adhesion layers on the printed Au nanoring arrays was confirmed by the XPS analysis, as seen in Figure S8. In the XPS patterns, two main peaks are detected at 465.02 and 459.62 eV, which correspond to the binding energies of Ti ($2p_{1/2}$) and Ti ($2p_{3/2}$), respectively. This clearly shows that the Ti layers strongly adhere to the interfaces between the printed Au nanorings and substrate surfaces.

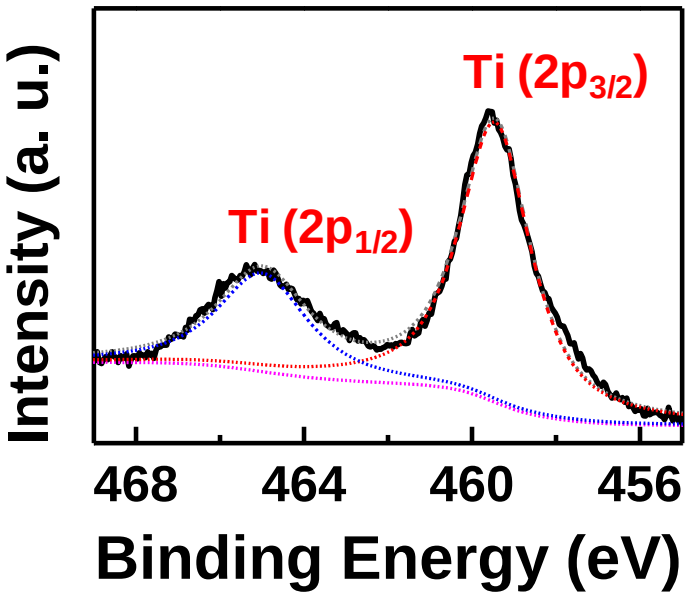

Figure S8. XPS patterns of the Ti adhesion-enhanced layers on the printed Au nanoring arrays.

The large range of XRD inspections:

The XRD patterns in Figure S9 show the large range of XRD inspection from 10^{o} to 80^{o} over the printed metal nanoring arrays of Figure 4 in the manuscript. In the XRD data, no other diffraction peaks, excluding the main peaks from the printed metal nanorings and substrates, were detected, indicating that various metal nanoring arrays were successfully formed on a wide range of substrate substances.

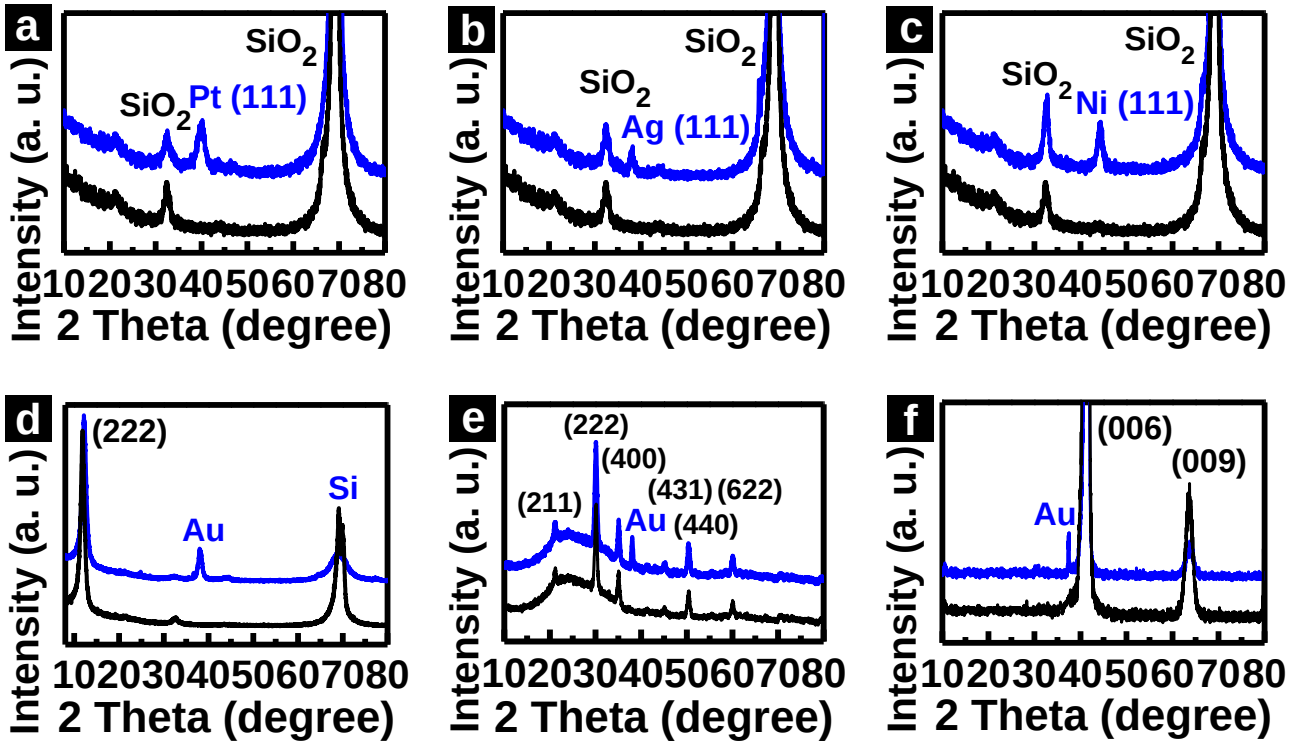

Figure S9. The XRD patterns of (a) Pt, (b) Ag, and (c) Ni nanoring arrays printed on SiO_2 substrates. The XRD inspections of Au nanorings printed on (d) graphene oxide layers dispersed over Si substrates, (e) ITO substrates, and (f) c-plane sapphire substrates.

LSPR of the printable Au nanodots and nanorings:

The SEM images in Figure S10a show the Au nanodot arrays that were printed on a quartz substrate by carbon nanopost arrays, which were used in our previous research to form sub-100 nm metal nanodots [*ACS Nano* **2011**, *5*, 5543-5551], while the images in Figure S10b show the Au nanoring arrays that were printed on a quartz substrate by the CNT stamps. These dots and rings exhibit almost the same size, interval, height, and density. The UV/Vis/NIR absorption patterns of the printable Au nanodots and nanorings in the center of Figure S9 indicate a considerable red-shift from the visible to NIR regions as the configuration of the Au nanostructures is changed from dots to rings, which might be due to the much stronger interaction of the rings between the outer disk and the inner cavity compared with the dots that have a disk configuration.

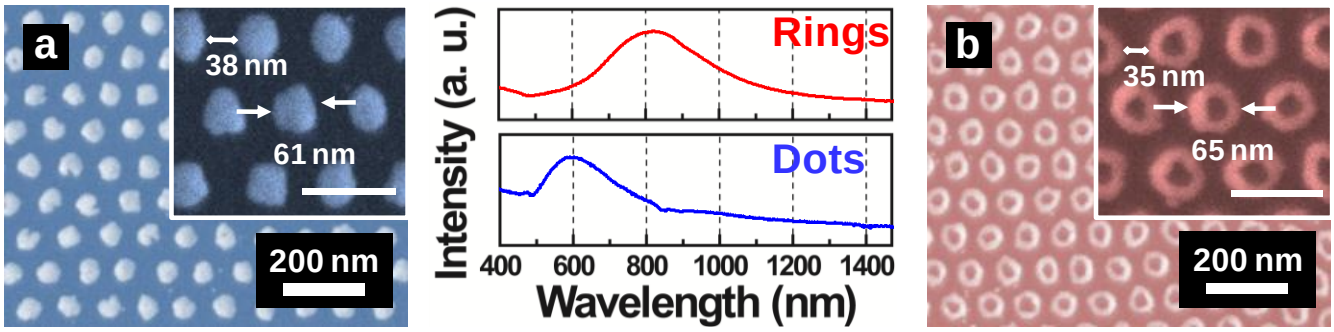

Figure S10. SEM images of the (a) Au nanodots and (b) Au nanorings that were printed on quartz substrates. The extinction patterns in the center of the figures show the different resonance spectra in accordance with the shapes (dots and rings) of the Au nanostructures. All of the scale bars in the inset images are 100 nm.